Revista Mexicana de Astronomía y Astrofísica, **59**, 191–200 (2023)
© 2023: Instituto de Astronomía, Universidad Nacional Autónoma de México
https://doi.org/10.22201/ia.01851101p.2023.59.02.04

© Copyright 2023: Instituto de Astronomía, Universidad Nacional Autónoma de México
DOI: https://doi.org/10.22201/ia.01851101p.2023.59.02.04

NEW SPECTROSCOPY OF U GEM

J. Echevarría[1], S. H. Ramírez[2], M. Fuentes[3], L. J. Sánchez[1], V. Patiño[4,5], and V. Chavushyan[4]

Received November 21 2022; accepted March 8 2023

ABSTRACT

We present new optical spectroscopic observations of U Geminorum obtained during a quiescent stage. We perform a radial velocity analysis of three Balmer emission lines yielding inconsistent results. Assuming that the radial velocity semi amplitude accurately reflects the motion of the white dwarf, we arrive at masses for the primary which are in the range of $M_{\rm wd} = 1.21 - 1.37 M_{\odot}$. Based on the internal radial velocity inconsistencies and results produced from the Doppler tomography – wherein we do not detect emission from the hot spot, but rather an intense asymmetric emission overlaying the disc, reminiscent of spiral arms – we discuss the possibility that the overestimation of the masses may be due to variations of gas opacities and a partial truncation of the disc.

RESUMEN

Presentamos nuevas observaciones espectroscópicas de U Geminorum obtenidas durante un estado de quietud. Realizamos un análisis de velocidades radiales para tres líneas de Balmer, cuyos resultados son inconsistentes. Asumiendo que la semi-amplitud de la velocidad radial refleja fielmente el movimiento de la componente primaria, obtuvimos valores de masa de la primaria en el intervalo $M_{\rm wd} = 1.21 - 1.37 M_{\odot}$. Basados en la inconsistencia de nuestros resultados y en las imágenes de tomografía Doppler – donde no detectamos emisión del punto caliente, sino que aparece una emisión sobrepuesta al disco, que asemeja brazos espirales– discutimos la posibilidad de que la sobreestimación de la masa sea debida a variaciones de las opacidades y a un disco truncado.

Key Words: novae, cataclysmic variables — stars: dwarf novae — stars: individual: U Gem — techniques: spectroscopic

1. INTRODUCTION

U Geminorum is the prototype of a subclass of dwarf novae (DN), which belong to the cataclysmic variable systems (CVs). These are semi-detached interactive binaries where the primary is a compact white dwarf (WD) accreting material from a Roche-lobe filling companion, which normally is a late type star very close to the main-sequence. According to the classical model developed by Smak (1971) and Warner & Nather (1971), the material accreted by the secondary star forms an annulus or ring in the outer regions due to its large amount of angular momentum, and eventually forms a full disc, down to the boundary of the WD, due to viscous forces within its layers. When the disc is well formed the material strikes the disc in the outer rim which results in a conspicuous bright spot. This region, also known as the hot spot, is observed as an orbital hump in the optical light-curves of U Gem during quiescence, which precedes an eclipse of the bright spot and a partial eclipse of the accretion disc.

U Gem has an orbital period of 0.1769061911 days and a mass ratio of $q = 0.35 \pm 0.05$ (Echevarría et al. 2007), with an inclination of $i = 69.7^{\circ} \pm 0.7^{\circ}$ (Zhang & Robinson 1987). It has an outburst recurrence of ≈ 118 days. Models from Takeo et al. (2021) predict that the inner disc is truncated in quiescence at a distance of $\approx 1.20 - 1.25$ times the WD radius, whereas in outburst it truncates at 1.012 $R_{\rm wd}$ or might even extend to the WD surface. The FUV

[1]Instituto de Astronomía, Universidad Nacional Autónoma de México, México.
[2]Department of Physics, University of Warwick, UK.
[3]Departamento de Física, Universidad de Sonora, Sonora, México.
[4]Instituto Nacional de Astrofísica, Óptica y Electrónica, Tonantzintla, Puebla, México.
[5]Max-Planck-Institut für Radioastronomie, Bonn, Germany.

© Copyright 2023: Instituto de Astronomía, Universidad Nacional Autónoma de México
DOI: https://doi.org/10.22201/ia.01851101p.2023.59.02.04

lightcurve analyzed by Godon et al. (2017) shows phase-dependent modulations which are consistent with a stream overflow of the disc.

Multiple radial velocity studies have been conducted on U Gem, from which the semi-amplitudes of the components have been derived. Tracing the $H\alpha$ Balmer emission line, Echevarría et al. (2007) obtained a radial velocity for the white dwarf of $K_1 = 107 \pm 2$ kms^{-1}, in agreement with the analyses of FUV observations put forward by Long & Gilliland (1999), who reported a value of $K_1 = 107.1 \pm 2.1$ kms^{-1}.

By means of Doppler tomography – a technique that analyzes the Doppler shifts of an emission line to obtain a two-dimensional distribution of the emission in accretion discs (Marsh & Horne 1988)– this object has been observed to exhibit diverse emission structures in quiescence: from that of an extended disc dominated by the emission from the hot spot (Echevarría et al. 2007; Marsh et al. 1990), to a highly asymmetric shape similar to spiral arms overlaying the disc (e.g. Unda-Sanzana et al. 2006; Neustroev & Borisov 1998).

Despite being one of the best studied DN, and a prototype object, U Gem continues to show a behaviour far more complicated than that contemplated in the classical model. Thus, it is an object worth of continuous monitoring. With this in mind, in § 2 we present optical spectroscopic observations of U Gem obtained during quiescence. § 3 is a radial velocity study of the system implemented on three distinct emission lines: Hβ, Hγ, and Hδ, by means of which the masses of the system are derived. § 4 consists of the discussion of the derived masses. It also includes an extensive discussion on the Doppler tomography obtained for the emission lines, which we used to find clues on the spatial origin of the emission within the disc. Finally, our conclusions are presented in § 5.

2. OBSERVATIONS AND REDUCTION

Spectra were obtained with the 2.1-m telescope of the Observatorio Astrofísico Guillermo Haro at Cananea, Sonora, using the Boller and Chivens spectrograph and a E2V42-40, 2048x2048 CCD detector in the 4000 - 5000 Å range with a resolution of R ≈ 1700, on the nights of 2021 February 15 and 16. The exposure time for each spectrum was 600 s. Standard IRAF[6] procedures were used to reduce the data.

[6]IRAF is distributed by the National Optical Astronomy Observatories, which are operated by the Association of Universities for Research in Astronomy, Inc., under cooperative agreement with the National Science Foundation.

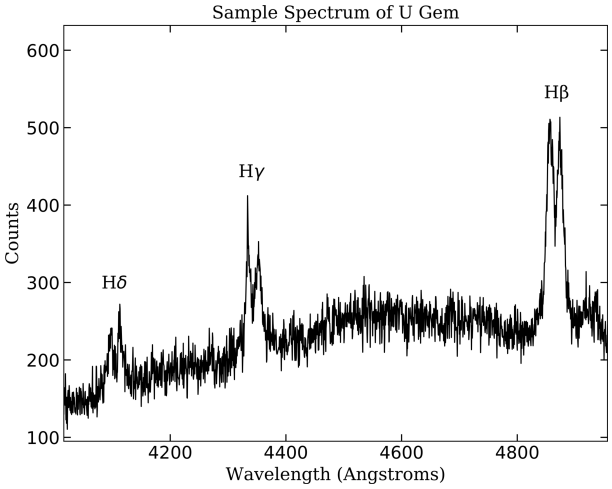

Fig. 1. Individual spectrum of U Gem showing the strong double-peaked Balmer lines.

TABLE 1

LOG OF SPECTROSCOPIC OBSERVATIONS OF U GEM

Date	Julian Date (2450000 +)	No. of spectra	Exp. Time
15 Feb 2021	9260	47	600 s
16 Feb 2021	9261	34	600 s

The log of observations is shown in Table 1. The spectra show strong double-peaked Balmer lines, as exhibited in the sample in Figure 1. The spectra are not flux calibrated, therefore the y-axis shows counts in each spectrum.

3. RADIAL VELOCITIES

The radial velocity of the emission lines of each spectrum was computed using the RVSAO package in IRAF, with the CONVRV function, developed by J. Thorstensen (2008, private communication). This routine follows the algorithm described by Schneider & Young (1980), convolving the emission line with an antisymmetric function, and assigning the centre of the line profile to the root of this convolution. As in Segura-Montero et al. (2020), we used the Double-Gaussian method (GAU2 option available in the routine), which uses a negative and a positive Gaussian to convolve the emission line. The algorithm uses as input the width and separation of the Gaussians. This method traces the emission of the wings of the line profile, presumably arising from the inner parts of the accretion disc.

Following the methodology described by Shafter et al. (1986), we made a diagnostic diagram to find

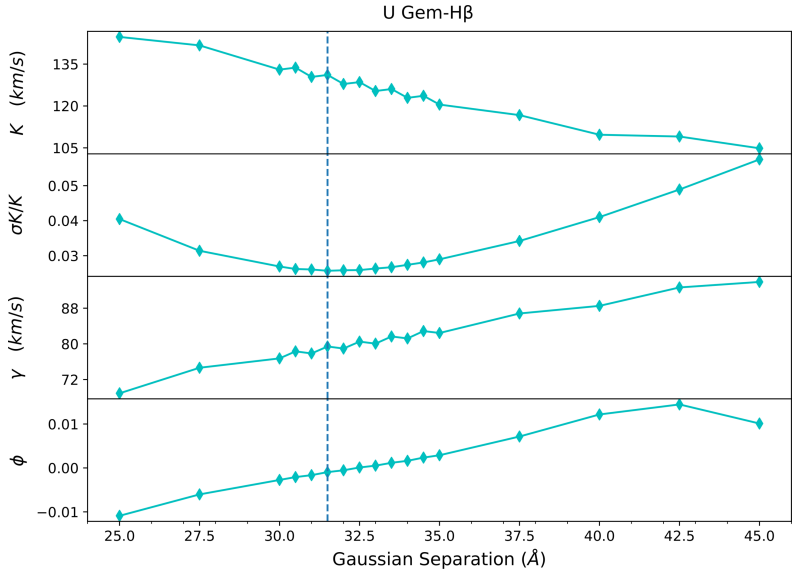

Fig. 2. Diagnostic diagram of the $H\beta$ emission line. The vertical blue dashed line indicates the best solution. See text for further discussion. The colour figure can be viewed online.

TABLE 2

ORBITAL PARAMETERS

Parameter	Hβ	Hγ	Hδ
γ (km s^{-1})	79.4 ± 2.3	81.2 ± 3.4	122.5 ± 4.9
K_1 (km s^{-1})	131.1 ± 3.3	110.0 ± 5.0	136.9 ± 7.1
HJD_0*	0.0077 ± 0.0006	0.005 ± 0.001	0.008 ± 0.001
P_{orb} (min)	Fixed**	Fixed**	Fixed**

*(2459261+ days).

**0.1769061911 days.

the optimal Gaussian separation, by fitting each trial to a simple circular orbit :

$$V(t) = \gamma + K_1 \sin\left(2\pi \frac{t - t_0}{P_{orb}}\right), \qquad (1)$$

where γ is the systemic velocity, K_1 the semi-amplitude (assumed to be the WD orbital velocity), t_0 the time of inferior conjunction of the donor and P_{orb} is the orbital period. We employed χ^2 as our goodness-of-fit parameter. Note that we have fixed the orbital period in our calculations, and therefore we only fit the other three orbital parameters. This is a convenient way to improve the fit of the remaining free parameters as the orbital period has been obtained from the eclipses of the object (e.g. Echevarría et al. 2007).

Constructing a diagnostic diagram requires an interactive fitting between the CONVRV routine and a program to fit the orbital parameters. We have used ORBITAL[7] a simple least squares program to determine, in general, the three free orbital parameters. In particular, a control parameter is defined in this diagnostic, σ_K/K, whose minimum is a very good indicator of the optimal fit. In our runs we have found that the best results are obtained with a relatively small width of about 10–15 pixels. The diagnostic diagram for $H\beta$ is displayed in Figure 2, while the orbital fit for its best solution is exhibited in Figure 3. The parameters yielded for the optimal orbital fit are shown in Table 2. In a similar way, we have constructed the diagnostic diagrams for $H\gamma$ and $H\delta$. These, and the corresponding best orbital fits, are shown in Figures 4 to 7, while the orbital parametrs are also shown in Table 2.

The radial velocity fit for the $H\beta$ and $H\delta$ emission lines yield consistent K_1 values within the er-

[7]Available at `https://github.com/Alymantara/orbital_fit`

© Copyright 2023: Instituto de Astronomía, Universidad Nacional Autónoma de México
DOI: https://doi.org/10.22201/ia.01851101p.2023.59.02.04

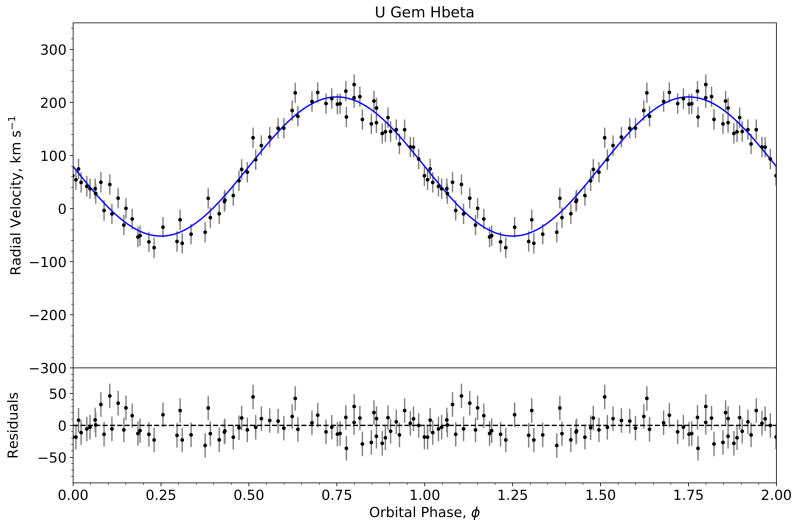

Fig. 3. Radial velocity curve for the best solution of the $H\beta$ emission line. The colour figure can be viewed online.

TABLE 3

BASIC SYSTEM PARAMETERS YIELDED BY THE K_1 AMPLITUDE VALUE OF EACH EMISSION LINE

Parameter	$H\alpha^{\dagger}$	Hβ	Hγ	Hδ
q	0.34 ± 0.01	0.42 $\pm$0.01	0.35 $\pm$0.01	0.44 $\pm$0.02
M_1 ($M_\odot$)	1.20 ± 0.05	1.34 $\pm$0.05	1.22 $\pm$0.06	1.38 $\pm$0.07
M_2 ($M_\odot$)	0.42 ± 0.04	0.57 $\pm$0.02	0.43 $\pm$0.03	0.61 $\pm$0.05
$a(R_\odot)$	1.55 ± 0.02	1.64 $\pm$0.02	1.56 $\pm$0.03	1.67 $\pm$0.03

†(Echevarría et al. 2007).

rors. They also agree with the value of $K_1 = 138 \pm 8$ kms^{-1}, obtained from an analysis of the same lines performed by Stover (1981). On the other hand $H\gamma$ agrees with the more accurate result of $K_1 = 107.1 \pm 2.1$ kms^{-1} obtained by Long & Gilliland (1999), who traced the Doppler shifts of the WD photospheric absorption lines in the FUV range; also in agreement with Echevarría et al. (2007), who followed the same methodology used in this paper, but applied to the $H\alpha$ Balmer emission line only ($K_1 = 107 \pm 2$ kms^{-1}).

4. DISCUSSION

4.1. *Basic System Parameters*

From the determination of the orbital parameters obtained in § 3 we can estimate the masses of the system components, as well as the binary separation, provided that an accurate estimation of the inclination angle is available. These mass estimates depend strongly on the assumption that the semi-amplitude derived from the emission lines accurately reflects the motion of the white dwarf, i.e. that the measurements of the wings of the lines are not distorted and present a symmetric behavior along the orbital period. The basic system parameters are obtained with the following formulae:

$$q = \frac{K_1}{K_2} = \frac{M_2}{M_1}, \tag{2}$$

$$M_1 \sin^3 i = \frac{PK_2(K_1 + K_2)^2}{2\pi G}, \tag{3}$$

$$M_2 \sin^3 i = \frac{PK_1(K_1 + K_2)^2}{2\pi G}, \tag{4}$$

$$a \sin i = \frac{P(K_1 + K_2)}{2\pi}, \tag{5}$$

where q is the mass ratio; M_1 is the mass of the primary; M_2 the mass of the secondary; i the inclination angle, K_1 and K_2 are the semi-amplitude of the primary and secondary, respectively; and a is the binary separation. To employ equations 2–5, we adopted the inclination derived by Zhang & Robinson (1987) of $i = 69.7° \pm 0.7°$ and the semi-amplitude of the secondary derived by Echevarría et al. (2007) of $K_2 = 310 \pm 5$ kms^{-1}.

Table 3 shows a summary for the system parameters yielded when using each of the K_1 values from

© Copyright 2023: Instituto de Astronomía, Universidad Nacional Autónoma de México
DOI: https://doi.org/10.22201/ia.01851101p.2023.59.02.04

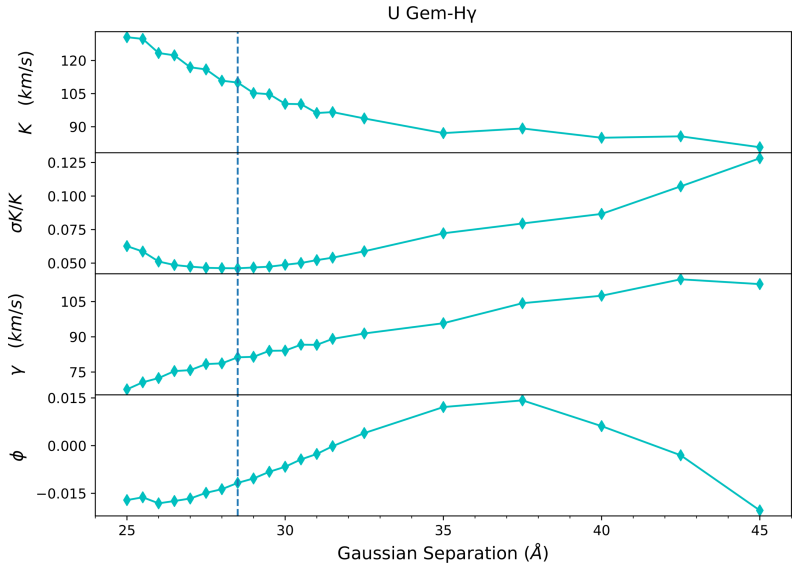

Fig. 4. Diagnostic diagram of the $H\gamma$ emission line. The vertical blue dashed line indicates the best solution. See text for further discussion. The colour figure can be viewed online.

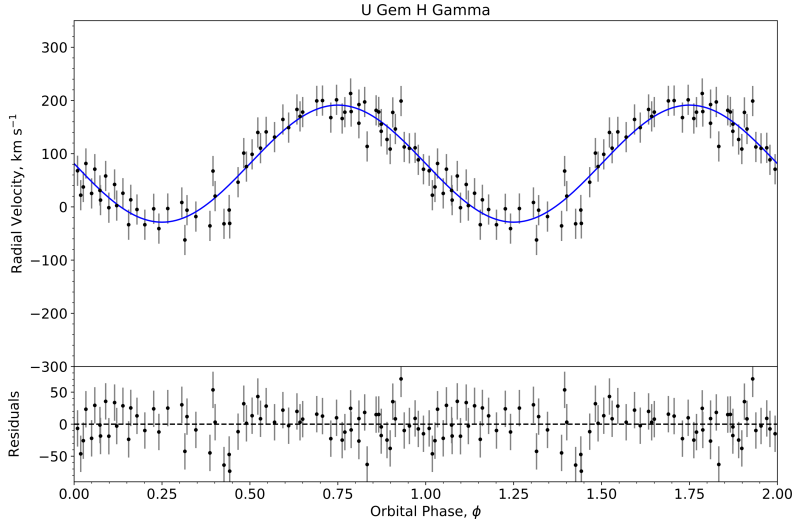

Fig. 5. Radial velocity curve for the best solution of the $H\gamma$ emission line. The colour figure can be viewed online.

the three lines, obtained in § 3. For comparison, we also include the parameters reported for $H\alpha$ by Echevarría et al. (2007).

As expected from the high K_1 values for Hβ and Hδ, and because we are using the same i and K_2 constraints as Echevarría et al. (2007), the system parameters for these lines resulted in an overestimation with respect to those obtained from the $H\alpha$ analysis of the aforementioned authors (See Table 3). On the other hand, the parameters yielded for $H\gamma$ are consistent with those reported by Echevarría et al. (2007), because of the agreement of the K_1 value.

A possible explanation for our radial velocity parameter overestimation and thus for our mass parameter calculations could be made based on the X-ray analysis of Takeo et al. (2021), whose models predict that the accretion disc is truncated at 1.25 Rwd during quiescence, as expected by the theory (Narayan & Popham 1993). Given that the Double-Gaussian method, employed in § 3, traces the inner region of the disc, this truncation could result in higher values for the radial velocity of the WD.

It is possible that the inner part of the disc does contain mass, but at such low density and low surface brightness that it is optically thin (e.g. Pringle

© Copyright 2023: Instituto de Astronomía, Universidad Nacional Autónoma de México
DOI: https://doi.org/10.22201/ia.01851101p.2023.59.02.04

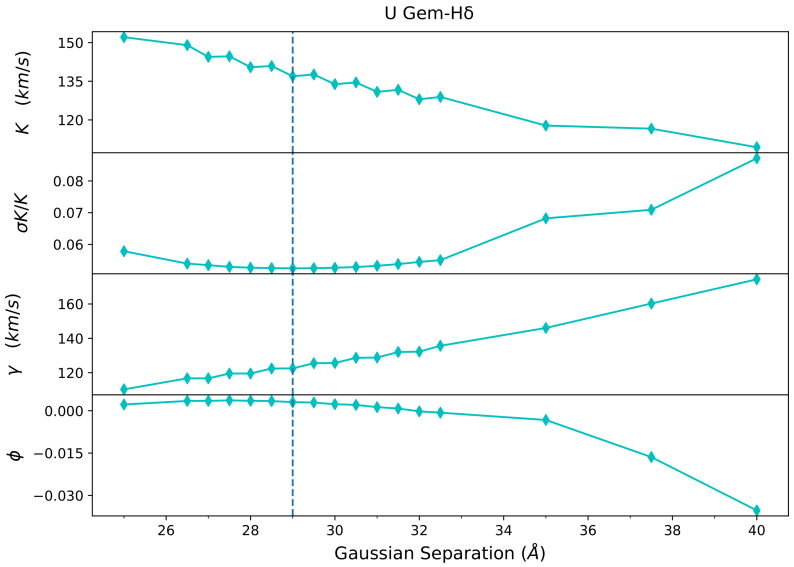

Fig. 6. Diagnostic diagram of the $H\delta$ emission line. The vertical blue dashed line indicates the best solution. See text for further discussion. The colour figure can be viewed online.

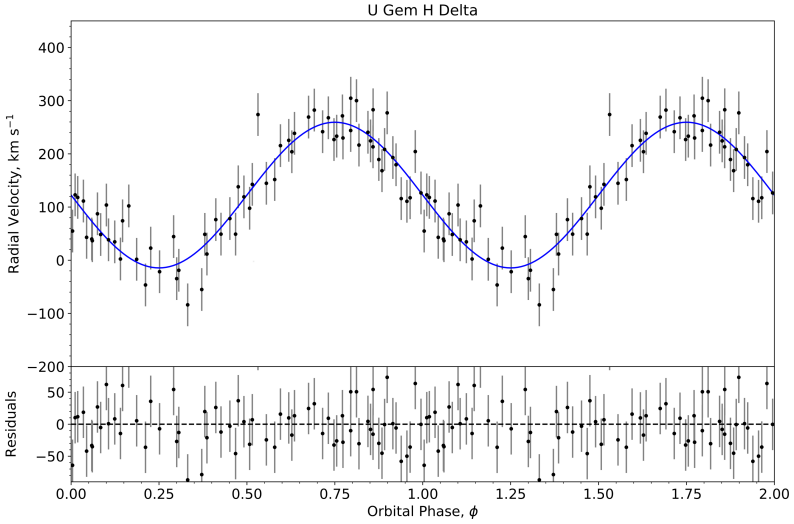

Fig. 7. Radial velocity curve for the best solution of the $H\delta$ emission line. The colour figure can be viewed online.

© Copyright 2023: Instituto de Astronomía, Universidad Nacional Autónoma de México
DOI: https://doi.org/10.22201/ia.01851101p.2023.59.02.04

1981). Furthermore, as explained in § 4.2, we detect an asymmetry overlaying the disc in our Doppler tomograms. These circumstances could imply abrupt variations of opacities within the disc, which would explain our internal inconsistencies in the radial velocity analysis (e.g. Mason et al. 2000).

4.2. *Doppler Tomography*

Doppler tomography is an indirect imaging technique developed by Marsh & Horne (1988). It produces two-dimensional mappings of the emission intensity in velocity space of the accretion disc, using the phase-resolved profiles of the spectral emission lines. We produced the Doppler tomography of the $H\beta$, $H\gamma$ and $H\delta$ Balmer emission lines, using a Python wrapper [8] (Hernandez Santisteban 2021) of the FORTRAN routines published by Spruit (1998) within an IDL environment. Figures 8-10, show the resulting images from the analysis, with the following layout: in the top left panel we show the observed trailed spectra; the tomography is displayed in the bottom panel; and the reconstructed trailed spectra, which are created by collapsing the tomography

[8] Available at `https://github.com/Alymantara/pydoppler`

© Copyright 2023: Instituto de Astronomía, Universidad Nacional Autónoma de México
DOI: https://doi.org/10.22201/ia.01851101p.2023.59.02.04

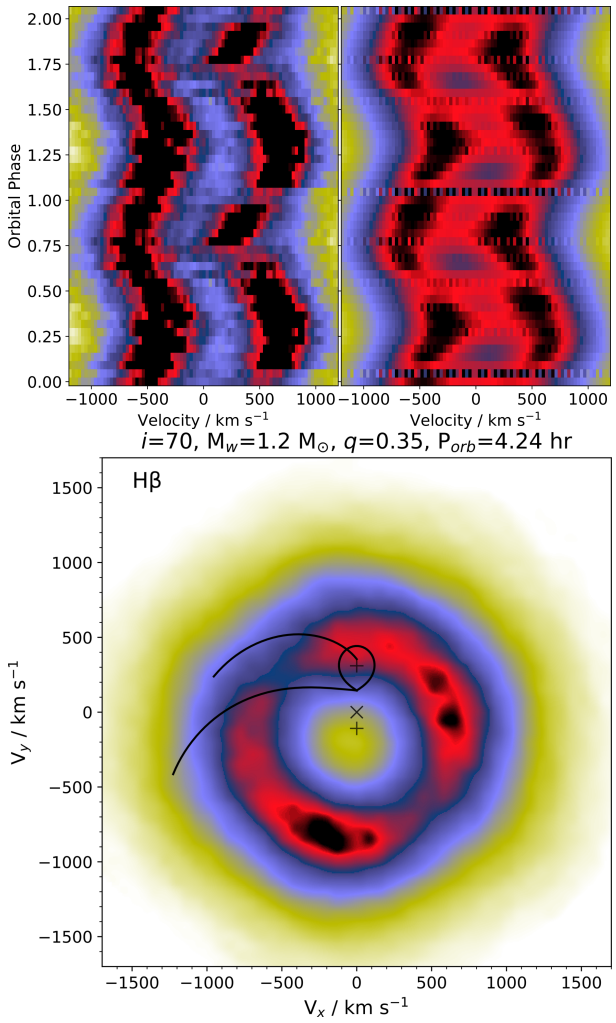

Fig. 8. Trail spectra and Doppler tomography of the $H\beta$ emission line. The relative emission intensity is shown in a scale of colours, where the strongest intensity is represented by black, followed by red, then blue, and finally yellow. The cross markings represent (from top to bottom) the position of the secondary, the centre of mass and the primary component. The Roche lobe of the secondary is depicted around its cross. The Keplerian and ballistic trajectories of the gas stream are marked as the upper and lower : curves, respectively. The colour figure can be viewed online.

image along the direction defined by the respective orbital phase (Marsh 2005), appear in the top right panel.

The trailed spectra of all three Balmer lines show a conspicuous double-peaked structure, characteristic of the line profiles of discs in systems of high inclination (Horne & Marsh 1986; Marsh & Horne 1988). The spectrograms exhibit an evident lack of a hot-spot signature, which would appear as an s-wave oscillating from peak to peak.

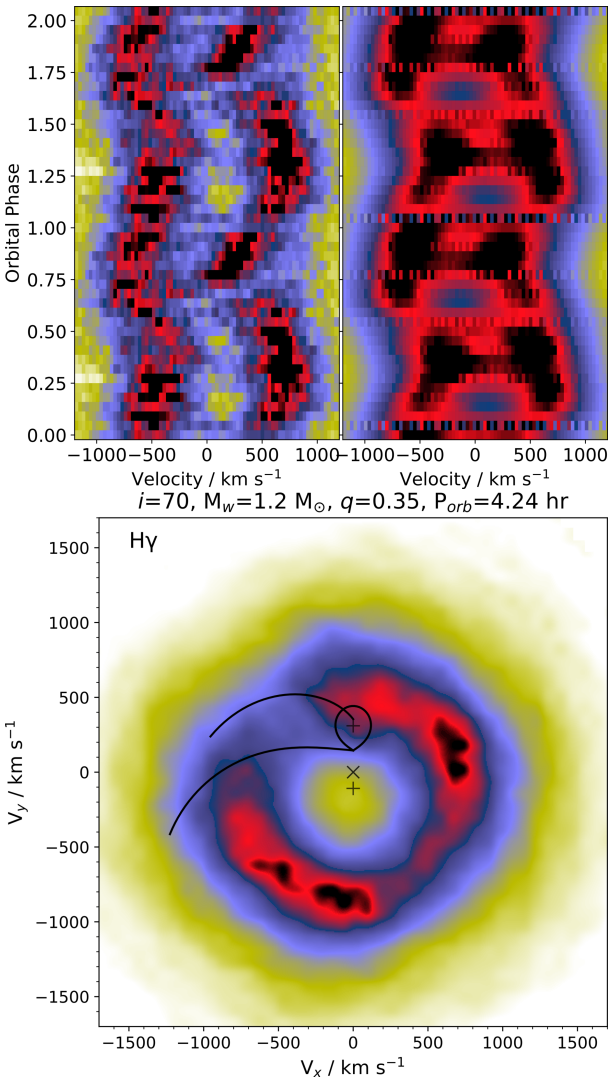

Fig. 9. Trail spectra and Doppler tomography of the $H\gamma$ emission line. The relative emission intensity is shown in a scale of colours, where the strongest intensity is represented by black, followed by red, then blue, and finally yellow. The cross markings represent (from top to bottom) the position of the secondary, the centre of mass and the primary component. The Roche lobe of the secondary is depicted around its cross. The Keplerian and ballistic trajectories of the gas stream are marked as the upper and lower curves, respectively. The colour figure can be viewed online.

The overall structure in our three tomography images is in contrast to most previous Doppler tomography studies of U Gem in quiescence, which were dominated by an intense emission corresponding to a hot spot component (e.g. Marsh et al. 1990; Echevarría et al. 2007). Instead, we find an asymmetric region of enhanced emission overlaying the disc, consistent with the structure exhibited by spiral

© Copyright 2023: Instituto de Astronomía, Universidad Nacional Autónoma de México
DOI: https://doi.org/10.22201/ia.01851101p.2023.59.02.04

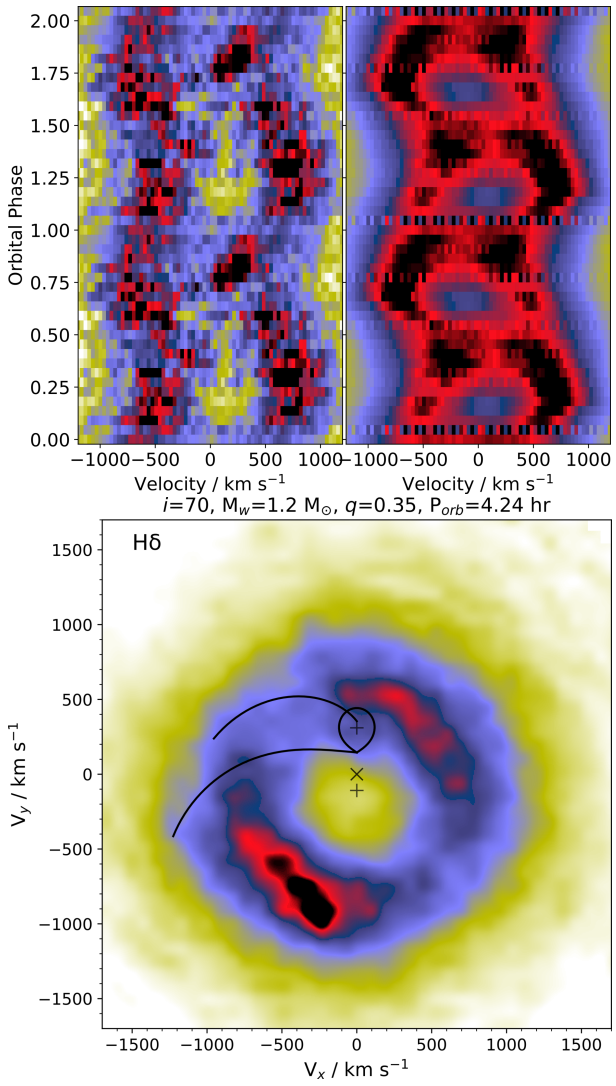

Fig. 10. Trail spectra and Doppler tomography of the $H\delta$ emission line. The relative emission intensity is shown in a scale of colours, where the strongest intensity is represented by black, followed by red, then blue, and finally yellow. The cross markings represent (from top to bottom) the position of the secondary, the centre of mass and the primary component. The Roche lobe of the secondary is depicted around its cross. The Keplerian and ballistic trajectories of the gas stream are marked as the upper and lower curves, respectively. The colour figure can be viewed online.

density waves (eg. Steeghs et al. 1997). While U Gem has been observed to show this structure in Doppler tomograms before (Neustroev & Borisov 1998; Unda-Sanzana et al. 2006), the presence of fully formed spiral shocks in U Gem must be regarded with caution: the study of the evolution of spiral shocks in U Gem performed by Groot (2001) shows that they fade during the decline of the outburst. And even if spiral arms were present in U Gem in quiescence, they would be expected to be tightly wrapped during this stage (Steeghs & Stehle 1999); hence very difficult to detect with Doppler tomography (Ruiz-Carmona et al. 2020). As discussed by Unda-Sanzana et al. (2006), the spiral feature in the tomography could instead be explained by irradiation from the WD of regions of the disc that become thickened from tidal distortion.

Nonetheless, our understanding of spiral shocks from 2D models has shown limitations before, as in the simulations by Godon et al. (1998) which predicted an unrealistically hot disc in order to reproduce the two-armed spiral pattern exhibited in the tomography of IP Peg by Steeghs et al. (1997). Moreover, a previous detection in quiescence makes the limitations evident: the Doppler maps reported by Pala et al. (2019) exhibit a clear signature of spiral shocks in a quiescent state of the WZ Sge object SDSS J123813.73-033933.0; confirmed by the double hump modulation of the white dwarf in their *HST* data, caused by the interface between the white dwarf and the inner edge of the spiral shocks. And since the mass ratio of U Gem, $q = 0.35 \pm 0.03$ (Echevarría et al. 2007), sets it right on the limit that allows the disc to achieve the 3:1 resonance ($q \lesssim 0.3$) (Hellier 2001), spiral arms cannot be completely discarded.

Another possible explanation is provided by Smak (2001), who argues that the high radial velocity of $K_1 = 138 \pm 8$ kms^{-1} obtained by Stover (1981) (in accordance with our own values yielded for $H\beta$ and $H\delta$) could be caused by stream overflow of the disc. This would explain the absence of a hot spot in our tomography images, since the stream overshoot would avoid (or ameliorate) the initial impact with the rim of the disc. Stream material overshooting the disc edge and re-impacting at radii with lower velocity can create a second hot spot (Lubow 1989) which usually shows up in regions within the lower quadrants of the Doppler tomograms, as is the case in SW Sextantis systems (Schmidtobreick 2017). This scenario is further supported by the phase-dependent modulation of the FUV light curve and absorption lines velocity reported by Froning et al. (2001), which can be explained by the stream overflowing the edge of the disc (Godon et al. 2017; Godon 2019).

In any case, it is puzzling that our tomography shows similar emission distributions for all three emission lines, implying that they arise from the same regions in the disc. This raises the question: why is it that for $H\beta$ and $H\delta$ we obtain values that are consistent with Stover (1981), which are

© Copyright 2023: Instituto de Astronomía, Universidad Nacional Autónoma de México
DOI: https://doi.org/10.22201/ia.01851101p.2023.59.02.04

likely corrupted by some additional effect on the disc; while on the other hand $H\gamma$ appears unaffected and agrees better with the more reliable WD radial velocity measured from *HST* FUV observations by Long & Gilliland (1999)? As mentioned in § 4.1, we expect this internal inconsistency to be caused by different gas opacities in the accretion disc (Mason et al. 2000), occurring as a consequence of some combination of the phenomena discussed above: WD irradiation of tidally thickened regions, stream overflow, a partially truncated disc, and perhaps even fully formed spiral arms.

However, this inconsistency is a clear example of the issues arising from measuring the radial velocity of the WD from optical data, even when presumably tracing the inner regions of the disc as is done in the Double-Gaussian method (see § 3).

5. CONCLUSIONS

We presented a spectroscopic analysis of the dwarf nova U Geminorum. We obtained the radial velocity of the system for three distinct Balmer emission lines: Hβ, Hγ, and Hδ, by tracing the outer regions of the profile (which arise from the inner sections of the accretion disc), with the purpose of obtaining the WD radial velocity K_1. The resulting semi-amplitude for Hγ is consistent with previous canonic results of $K_1 = 107.1 \pm 2.1$ kms^{-1} (Echevarría et al. 2007; Long & Gilliland 1999). However, the other two lines show a considerable discrepancy, agreeing instead with the value obtained by Stover (1981) of $K_1 = 138 \pm 8$ kms^{-1}. We expected to find the source of this inconsistency in the Doppler tomography study, but the tomograms show that all three lines arise from the same region. However, it must be noted that the tomography does not show a typical disc: in particular there is no evidence whatsoever of a hot spot; instead it exhibits a spiral arm structure unexpected for a system in quiescence. This unusual shape (which can be a product of stream overflow, WD irradiation or actual spiral arms), along with a partial truncation of the inner regions of the disc, could together amount to considerable differences of gas opacities within the accretion disc, which could explain the different values of K_1 obtained for our three emission lines (e.g. Mason et al. 2000).

U Gem stands as one of the best studied DN. However, as it is made evident in this paper, more ingredients than those prescribed by the classical model must come into play to better explain its behaviour. Therefore, we propose further observations of this source to help shed light on the mechanisms giving rise to its rich and interesting nature.

The authors are indebted to DGAPA (Universidad Nacional Autónoma de México) support, PAPIIT Projects IN114917 and IN103120. This project has received funding from the European Research Council (ERC) under the European Union's Horizon 2020 research and innovation programme (Grant Agreement No. 101020057). This work was supported by CONACyT (Consejo Nacional de Ciencia y Tecnología) Research Grants 280789 and 320987. This work was supported by the MPlfR-Mexico Max Planck Partner group led by V.M.P.-A. We thank the staff at the Observatorio Astrofísico Guillermo Haro for facilitating and helping us to obtain our observations. This research made extensive use of ASTROPY, a community-developed core Python package for Astronomy (Astropy Collaboration et al. 2013), Python's SciPy signal processing library (Virtanen et al. 2020), and MATPLOTLIB (Hunter 2007).

REFERENCES

Astropy Collaboration, Robitaille, T. P., Tollerud, E. J., et al. 2013, A&A, 558, 33, https://doi.org/10.1051/0004-6361/201322068

Echevarría, J., de la Fuente, E., & Costero, R. 2007, AJ, 134, 262, https://doi.org/10.1086/518562

Froning, C. S., Long, K. S., Drew, J. E., Knigge, Ch., & Proga, D. 2001, ApJ, 562, 963, https://doi.org/10.1086/323860

Godon, P., Livio, M., & Lubow, S. 1998, MNRAS, 295, 11, https://doi.org/10.1046/j.1365-8711.1998.29510584.x

Godon, P., Shara, M. M., Sion, E. M., & Zurek, D. 2017, ApJ, 850, 146, https://doi.org/10.3847/1538-4357/aa9616

Godon, P. 2019, ApJ, 870, 112, https://doi.org/10.3847/1538-4357/aaf3a2

Groot, P. J. 2001, ApJ, 551, 89, https://doi.org/10.1086/319826

Hameury, J. M. & Lasota, J. P. 2017, A&A, 602, 102, https://doi.org/10.1051/0004-6361/201730760

Hellier, C. 2001, Cataclysmic Variable Stars (Springer)

Hernandez Santisteban, J. V. 2021, PyDoppler: Wrapper for Doppler Tomography Software, ascl.soft 06003H

Horne, K. & Marsh, T. R. 1986, MNRAS, 218, 761, https://doi.org/10.1093/mnras/218.4.761

Hunter, J. D. 2007, CSE, 9, 90, https://doi.org/10.1109/MCSE.2007.55

Long, K. S. & Gilliland, R. L. 1999, ApJ, 511, 916, https://doi.org/10.1086/306721

Lubow, S. H. 1989, ApJ, 340, 1064, https://doi.org/10.1086/167458

Marsh, T. R. & Horne K. 1988, MNRAS, 235, 269, https://doi.org/10.1093/mnras/235.1.269

Marsh, T. R., Horne, K., Schlegel, E. M., Honeycutt, R. K., & Kaitchuck, R. M. 1990, ApJ, 364, 637, https://doi.org/10.1086/169446

Marsh, T. R. 2005, Ap&SS, 296, 403, https://doi.org/10.1007/s10509-005-4859-3
Mason, E., Skidmore, W., Howell, S. B., et al. 2000, MNRAS, 318, 440, https://doi.org/10.1046/j.1365-8711.2000.03780.x
Narayan, R. & Popham, R. 1993, Natur, 362, 820, https://doi.org/10.1038/362820a0
Neustroev, V. V. & Borisov, N. V. 1998, A&A, 336, 73, https://doi.org/10.48550/arXiv.astro-ph/9807076
Neustroev, V.V., Zharikov, S.V. & Borisov, N.V. 2016, A&A, 585, 10, https://doi.org/10.1051/0004-6361/201526363
Pala, A. F., Gänsicke, B. T., Marsh, T. R., et al. 2019, MNRAS, 483, 1080, https://doi.org/10.1093/mnras/sty3174
Patterson, J., Thorstensen, J. R., Vanmunster, T., et al. 2004, PASP, 116, 516, https://doi.org/10.1086/421034
Pringle, J. E. 1981, ARA&A, 19, 137, https://doi.org/10.1146/annurev.aa.19.090181.001033
Rodríguez-Gil, P., Gänsicke, B. T., Araujo-Betancor, S., et al. 2004, MNRAS, 349, 367, https://doi.org/10.1111/j.1365-2966.2004.07512.x
Ruiz-Carmona, R., Groot, P. J., & Steeghs, D. 2020, MNRAS, 491, 2217, https://doi.org/10.1093/mnras/stz2992
Schneider, D. P. & Young, P. 1980, ApJ, 238, 946, https://doi.org/10.1086/158059
Segura-Montero, O., Ramírez, S & Echevarría, J. 2020, MNRAS, 494, 4110, https://doi.org/10.1093/mnras/staa856
Schmidtobreick, L. 2017, arXiv:1705.09332, https://doi.org/10.48550/arXiv.1705.09332
Shafter, A. W., Szkody, P., & Thorstensen, J. R. 1986, ApJ, 308, 765, https://doi.org/10.1086/164549
Smak, J. 1971, AcA, 21, 15
Smak, J. 2001, AcA, 51, 279
Smak, J. & Waagen, E. O. 2004, AcA, 54, 433
Spruit, H. C. 1998, arXiv: astro-ph/9806141, https://doi.org/10.48550/arXiv.astro-ph/9806141
Steeghs, D., Harlaftis, E. T., & Horne, K. 1997, MNRAS, 290, 28, https://doi.org/10.1093/mnras/290.2.L28
Steeghs, D. & Stehle, R. 1999, MNRAS, 307, 99, https://doi.org/10.1046/j.1365-8711.1999.02634.x
Stepanyan, D. A. 1982, PZ, 21, 691
Stover, R. J. 1981, ApJ, 248, 684, https://doi.org/10.1086/159193
Takeo, M., Hayashi, T., Ishida, M., et al. 2021, PASJ, 73, 143, https://doi.org/10.1093/pasj/psaa111
Unda-Sanzana, E., Marsh, T. R., & Morales-Rueda, L. 2006, MNRAS, 369, 805, https://doi.org/10.1111/j.1365-2966.2006.10336.x
Virtanen, P., Gommers, R., Oliphant, T. E., et al. 2020, NatMe, 17, 261, https://doi.org/10.1038/s41592-019-0686-2
Warner, B. 1995, Cataclysmic Variable Stars, (Cambridge University Press)
Warner, B. & Nather, R. E. 1971, MNRAS, 152, 219, https://doi.org/10.1093/mnras/152.2.219
Zhang, E. H. & Robinson, E. L. 1987, ApJ, 321, 813, https://doi.org/10.1086/165674

© Copyright 2023: Instituto de Astronomía, Universidad Nacional Autónoma de México
DOI: https://doi.org/10.22201/ia.01851101p.2023.59.02.04

V. Chavushyan and V. Patiño: Instituto Nacional de Astrofísica, Óptica y Electrónica, Luis Enrique Erro #1, Tonantzintla, Puebla 72840, México.
J. Echevarría and L. J. Sánchez[1]: Instituto de Astronomía, Universidad Nacional Autónoma de México, Apartado Postal 70-264, Ciudad Universitaria, México D.F., C.P. 04510, México.
M. Fuentes: Departamento de Física, Universidad de Sonora, Unidad Regional Centro, Hermosillo, Blvd. Luis Encinas J, Calle Av. Rosales S/N, Centro, 83000, Sonora, México.
V. Patiño: Max-Planck-Institut für Radioastronomie, Auf dem Hügel 69, D-53121 Bonn, Germany.
S. H. Ramírez: Department of Physics, University of Warwick, Coventry CV4 7AL, UK.